

## Electronic Supporting Information

# Vibrational properties of isotopically enriched materials: the case of calcite

Ben Xu, Anna Hirsch, Leor Kronik, and Kristin M. Poduska

### Calculated Structural Parameters of Calcite

**Table S1** Experimental and computationally optimized parameters of the calcite hexagonal unit cell. Distances are in Å and volume in Å<sup>3</sup>. Experimental data are from Maslen, E. N.; Streltsov, V. A.; Streltsova, N. R. *Acta Crystallogr., Sect. B: Struct. Sci.* **1993**, 49, 636-641

	Exp.	calculated	% error
<i>a</i>	4.99	5.05	1.2
<i>c</i>	17.06	17.23	1.0
<i>V</i>	386.1	380.9	1.3
<i>d</i> <sub>C-O</sub>	1.28	1.30	1.6
<i>d</i> <sub>Ca-O</sub>	2.36	2.39	1.3

### Calculated and experimental peak positions shifts due to isotopic substitution

**Table S2** Experimental and calculated (PBE) peak position shifts due to isotopic substitutions. Shifts correspond to the change in peak position between minimum <sup>13</sup>C (0% for PBE calculations, or natural abundance (1%) in experiments) to a nominal 100% <sup>13</sup>C substitution. For the *v*<sub>3</sub> mode and the *v*<sub>2</sub> mode, the <sup>13</sup>C and <sup>12</sup>C peaks are distinct at intermediate substitution levels, so we also report the average value of the wavenumber split between the two isotopic peaks for intermediate substitution ranges. For the *v*<sub>4</sub> mode, there is no isotopically related split visible, so there are no values for intermediate substitution ranges displayed in this table. Uncertainty estimates are ±2 cm<sup>-1</sup> for all experimental values.

	<i>v</i> <sub>3</sub> shift		<i>v</i> <sub>2</sub> shift		<i>v</i> <sub>4</sub> shift	
	Expt.	PBE	Expt.	PBE	Expt.	PBE
max, min <sup>13</sup> C content	35	39	29	25	2	2
intermediate <sup>13</sup> C content (average split)	38	36	27	25	–	–

## Experimental Raman spectra

To complement our IR data, typical Raman spectra for calcite powders over the same range of isotopic compositions are shown in Figure S8. Raman spectra were obtained using a Renishaw inVia Raman Microscope 90Q314 with a Renishaw HPNIR830 laser source (633 nm, maximum power 500 mW), using a range of 2000-100  $\text{cm}^{-1}$ . IR and Raman spectroscopy obey different selection rules. Specifically, the  $\nu_2$  and  $\nu_3$  modes of calcite are not Raman active, whereas the  $\nu_1$  and  $\nu_4$  modes are. Thus, the  $\nu_4$  mode is the only mode for which comparison between Raman and IR spectra is possible. For this peak, we observe a shift to lower wavenumbers with increasing  $^{13}\text{C}$  content in both IR spectra (main text, Fig. 2d) and Raman spectra (Fig. S8c). The other three Raman peaks ( $\nu_1$  and two lattice modes in Fig. S8b,d,e) do not show significant variation with isotopic composition changes.

We note that the lattice modes shown in the Raman spectra in Figure S1 occur at wavenumbers (280  $\text{cm}^{-1}$  and 150  $\text{cm}^{-1}$ ) that are far below the detection range of mid-IR spectrometers (due to inherent limitations with window and beamsplitter transparencies below 350  $\text{cm}^{-1}$ ). Thus, our experiments did not explore the effect of isotopic substitutions on calcite lattice modes in the IR.

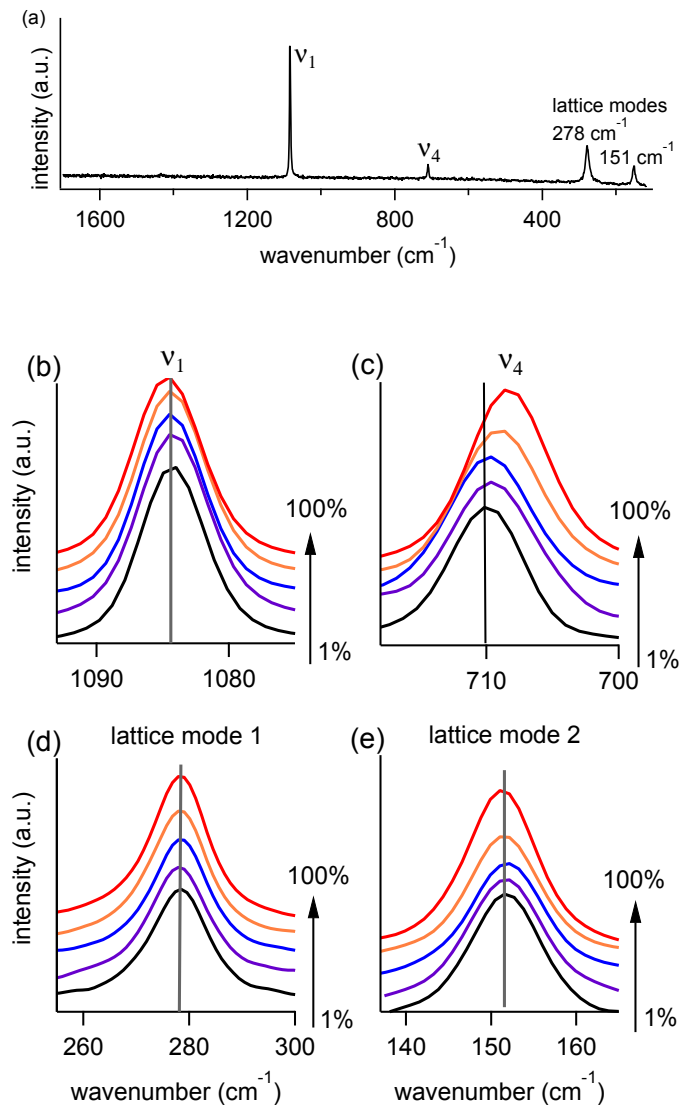


**Fig. S8** Raman spectra for calcite. (a) shows natural  $^{13}\text{C}$  abundance (1%), featuring two sharp peaks corresponding to the  $\nu_1$  and  $\nu_4$  vibrational modes (1084 and 710  $\text{cm}^{-1}$ , respectively) and two broader peaks related to lattice modes. (b)-(e) show expanded views of the four main modes, with vertical lines as a guide to the eye for peak positions at 1% isotope concentration. Nominal  $^{13}\text{C}$  concentrations are 1% (black), 13% (purple), 25% (blue), 50% (orange), and 100% (red). Only the  $\nu_4$  peak (c) shifts to lower wavenumbers upon isotope substitution.

### Computational studies of $^{13}\text{C}$ Isotopic Substitution: Additional Details

Table S3 summarizes the different structures which were constructed by replacing  $^{12}\text{C}$  atoms by  $^{13}\text{C}$  atoms in the conventional unit cell of calcite.

**Table S3** Summary of different  $^{13}\text{C}$  contents used for calculations.

# of $^{13}\text{C}$ replaced atoms	$^{13}\text{C}$ %
0	0
1*	8
1	17
2	33
3	50
4	67
5	83
6	100

\* Obtained by using a supercell consisting of two calcite hexagonal cells along the  $c$  axis.

Due to periodic boundary conditions, substitution of one  $^{13}\text{C}$  atom in the conventional hexagonal unit cell will result in a full-layer substitution in the crystal. In order to examine the influence of different configurations of atoms that are not part of the same layer, we used additional computational systems: an hexagonal  $2\times 2\times 1$  supercell and a rhombohedral  $2\times 2\times 2$  supercell. For both these supercells structures, it is possible to start from one atom in a layer and then, by addition of  $^{13}\text{C}$  atoms one at a time to the same layer, continue until the whole layer contains only  $^{13}\text{C}$  atoms (maximum of four). When the whole layer is substituted by  $^{13}\text{C}$  atoms, the supercell model reduces to the unit cell model. The calculated IR spectrum of the substituted supercell shown in Fig. S9. As expected, the addition of  $^{13}\text{C}$  atoms to the layer result in an increase of the intensity of the  $^{13}\text{C}$  peaks. Additionally, the positions of the  $\nu_3$  and  $\nu_2$  modes also change with a larger isotope content, resulting in a larger splitting between the  $^{12}\text{C}$  and  $^{13}\text{C}$  peak maxima.

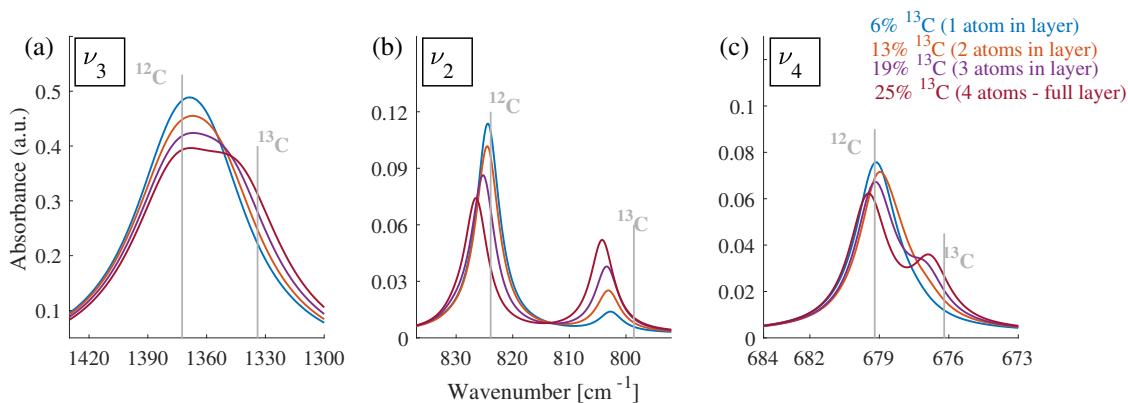


**Fig. S9** Comparison of calculated IR spectra for a rhombohedral supercell with different numbers of substituted  $^{13}\text{C}$  atoms within one layer. Vertical lines serve as guides to the eye for peak positions at 0% and 100%  $^{13}\text{C}$  concentrations.

Next, we examine the influence of isotope proximity on the calcite spectrum for a supercell structure, which allows for lower isotope concentrations compared with the conventional hexagonal unit cell (8% vs. 33%  $^{13}\text{C}$ ). We first substitute one isotope atom in the center of the supercell (4%  $^{13}\text{C}$  = 1 atom). For the hexagonal  $2\times 2\times 1$  super cell, one substituted isotope atom will have only  $^{12}\text{C}$  atoms as 1<sup>st</sup> neighbours. For substitution of two isotope atoms, their proximity arrangement can be chosen to be either 1<sup>st</sup>, 2<sup>nd</sup> or 3<sup>rd</sup> neighbors (8%  $^{13}\text{C}$  = 2 atom). The IR spectra corresponding to these configurations are shown in Fig. S10 and show that the line broadening can obscure subtle differences among the spectra. In the top row spectra, we show that setting the full-width half-maximum (FWHM) to half of the experimental value (which is a broadening similar to that used in all calculated spectra presented in the main text) yields no meaningful differences among the different configurations. However, when the FWHM is reduced to one quarter of the experimental broadening (lower row spectra), differences emerge for the  $\nu_3$  peak, which are consistent with the spectra shown in Fig. 4 in the main text. Therefore, the supercell IR spectra suggest that the discussed spectral changes due to isotopic proximity arrangements occur also at lower isotopic content, although are not always experimentally accessible.

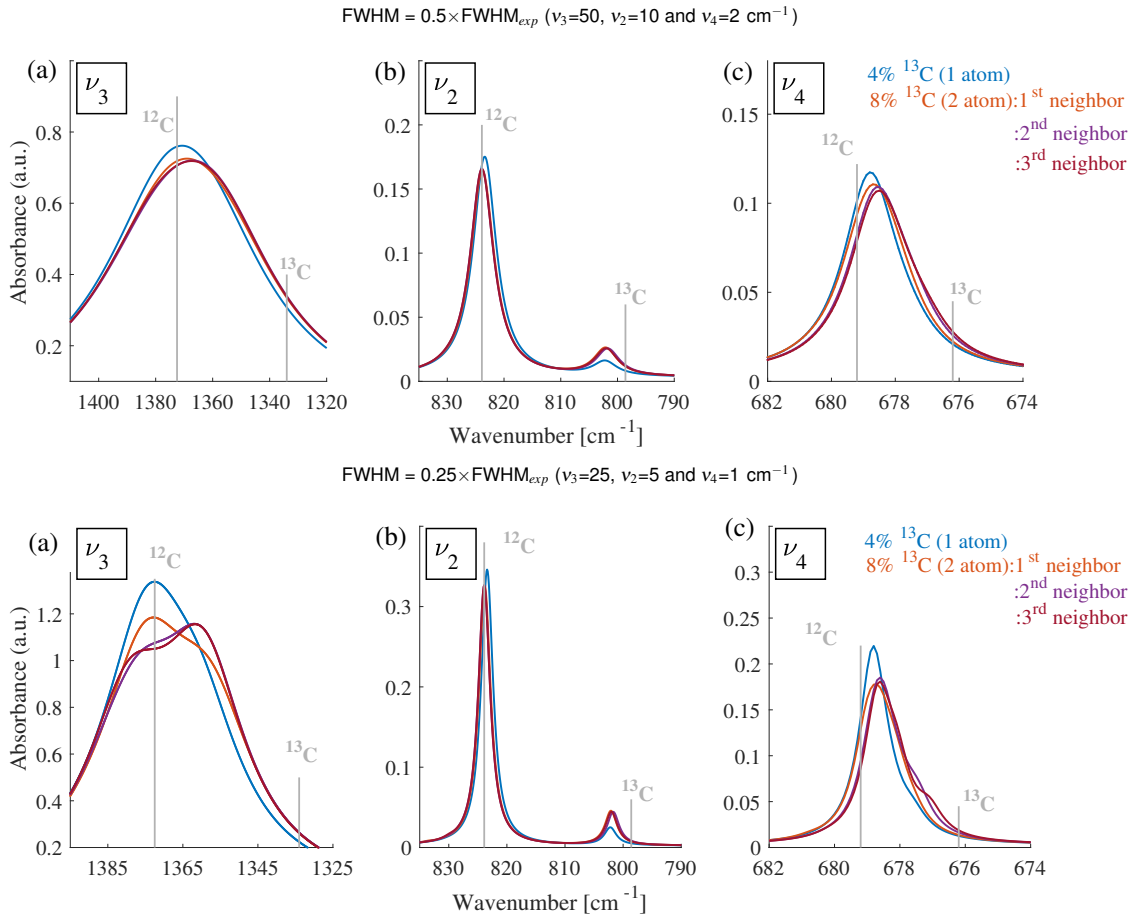


**Fig. S10** Comparison of calculated IR spectra for the hexagonal supercell with different numbers of substituted  $^{13}\text{C}$  atoms, with the proximity between the substituted atoms being either 1<sup>st</sup>, 2<sup>nd</sup>, or 3<sup>rd</sup> neighbors. The spectra are simulated with two different amounts of broadening:  $\text{FWHM}=0.5 \times \text{FWHM}_{\text{exp}}$  (top) and  $\text{FWHM}=0.25 \times \text{FWHM}_{\text{exp}}$  (bottom). Vertical lines serve as guides to the eye for peak positions at 0% and 100%  $^{13}\text{C}$  concentrations.

## LO-TO Splitting Additional Details

**Table S4** Calculated LO and TO frequencies (in  $\text{cm}^{-1}$ ) for 0%, 17% and 100%  $^{13}\text{C}$  isotope content

		0% $^{13}\text{C}$		17% $^{13}\text{C}$				100% $^{13}\text{C}$	
			$\Delta_{\text{LO-TO}}$	$^{12}\text{C}$	$\Delta_{\text{LO-TO}}$	$^{13}\text{C}$	$\Delta_{\text{LO-TO}}$	$\Delta_{\text{LO-TO}}$	
$\nu_3$	LO	1512	140	1507	133	1353	8	1471	138
	TO	1371		1374		1344		1333	
$\nu_2$	LO	839	14	838	12	809	3	814	15
	TO	825		826		806		799	
$\nu_4$	LO	681	2	680	1	677	0	679	2
	TO	679		679		677		677	

**Table S5** Comparison of LO-TO splitting frequencies (in  $\text{cm}^{-1}$ ) for calcite (0%  $^{13}\text{C}$ ), based on this work and previous experimental and computational results by others. Experiment results from Hellwege, K. H.; Lesch, W.; Plihal, M.; Schaack, G.Z. *Phys. A-Hadron. Nucl.*, **1970**, 232, 61-86. Computational (B3LYP) results from Valenzano, L.; Noel, Y.; Orlando, R.; Zicovich-Wilson, C. M.; Ferrero, M.; Dovesi, R. *Theor. Chem. Acc.* **2007**, 117, 991-1000

		This work (PBE)	$\Delta_{\text{LO-TO}}$	Exp.	$\Delta_{\text{LO-TO}}$	Calc. (B3LYP)	$\Delta_{\text{LO-TO}}$
$\nu_3$	LO	1512	140	1549	142	1554	154
	TO	1371		1407		1400	
$\nu_2$	LO	839	14	890	18	894	20
	TO	825		872		874	
$\nu_4$	LO	681	1	715	3	713	1
	TO	679		712		712	